# Stable Compositions and Structures of Copper Oxide Cluster Cations CunOm+ (n = 2-8) Studied by Ion Mobility Mass Spectrometry

# Stable Compositions and Structures of Copper Oxide Cluster Cations Cu$_n$O$_m^+$ (n = 2−8) Studied by Ion Mobility Mass Spectrometry

M. Abdul Latif, Jenna W. J. Wu, Ryoichi Moriyama, Motoyoshi Nakano, Keijiro Ohshimo, and Fuminori Misaizu*

Department of Chemistry, Graduate School of Science, Tohoku University, 6-3 Aoba, Aramaki, Aoba-ku, Sendai 980-8578, Japan

Ⓢ Supporting Information

**ABSTRACT:** Stable compositions and structures of copper oxide cluster cations have been studied by ion mobility mass spectrometry (IMMS) and density functional theory calculations. Cluster ions of the series Cu$_n$O$_m^+$ were predominantly observed with $n{:}m \approx 2{:}1$ in the mass spectrum. Collision cross sections (CCSs) of the cluster ions with $n{:}m \approx 2{:}1$, determined by IMMS, were found to increase monotonically with cluster size. In addition, the CCSs of Cu$_n$O$_n^+$ and Cu$_n$O$_{n-1}^+$ ($n = 2-8$) were examined, and stepwise increases were observed for Cu$_n$O$_{n-1}^+$ series. These cluster structures were assigned by comparison of the CCSs obtained via the IMMS experiment with theoretical orientation-averaged CCSs of optimized structures.
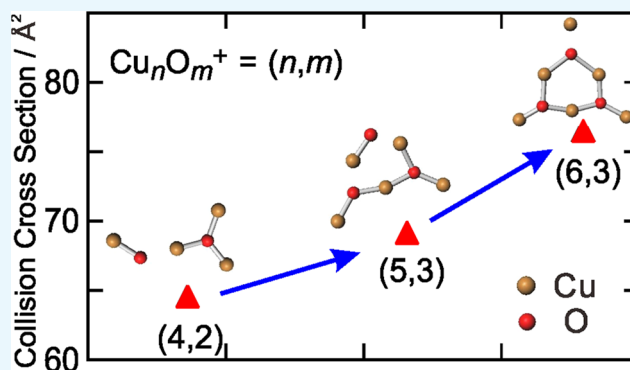
## 1. INTRODUCTION

Copper oxides exist as stable Cu$_2$O(I) and CuO(II) in the bulk phase. These copper oxides are widely used in various catalytic reactions,[1−5] semiconducting materials,[6,7] environmental protection,[8−11] and energy storage and conversion[12,13] systems. Understanding the properties of copper oxide surfaces may us help to elucidate their reactivity for different purposes. One of the fundamental ways to elucidate the behavior of the surface structures and details of their functional mechanism is to study gas-phase clusters. Such studies of copper oxide clusters give valuable insights into stabilities and reactions at the microscopic level, allowing size, stoichiometry, and oxidation states of the clusters to be selected according to research objectives. The geometrical structures of copper oxide clusters are the key parameters for understanding the catalytic reactivity of surface redox reactions. Moreover, information on structural changes that occur with varying cluster size is also valuable in application, because nanosized materials are expected to have functions that depend on their geometrical structures. Keeping these points in mind, many researchers have studied gas-phase copper oxide clusters during the past few decades.[14−22]

Experimentally, copper oxide cluster cations have been studied by mass spectrometry (MS) to determine the distributions of its sizes and compositions.[14−17] More explicitly, Freiser et al. investigated collision-induced dissociation (CID) of Cu$_n$O$_m^\pm$ cluster ions produced by laser desorption/ionization of copper oxide pellets.[14] Aubriet et al.,[15] Ma et al.,[16] and Mafuné et al.[17] determined the compositions of copper oxide cluster cations generated by laser ablation processes. They presented the stoichiometric compositions as an oxygen-deficient class, Cu$_n$O$_m^+$ ($n > m$),

such as Cu$_2$O$^+$, Cu$_3$O$^+$, Cu$_4$O$_2^+$, Cu$_5$O$_{2−3}^+$, Cu$_6$O$_{3−4}^+$, etc. Moreover, recently Hirabayashi and Ichihashi[18] and Mafuné et al.[19] reported the reactions of Cu$_n$O$_m^+$ cluster species with NO. They found that the Cu$_n$O$_m^+$ cluster ions readily react with NO and that the NO oxidation proceeds in the reaction with some specific sizes of clusters, such as Cu$_4$O$_3^+$, Cu$_6$O$_5^+$, etc.[18] For further investigations, a number of theoretical studies were also done mainly on compositional growth and their structures. Jadraque and Martín reported theoretical calculations for stable structures of the (Cu$_2$O)$_{n/2}^+$ and [(Cu$_2$O)$_{(n-1)/2}$Cu]$^+$ series, which were considered to consist of Cu$_2$O as a building block.[20] Yang et al. studied the ground-state structures of small copper oxide clusters, Cu$_2$O$_m$ ($m = 1-4$), through density functional theory (DFT) calculations[21] and found linear or near-linear structures. Hall et al. investigated copper oxide cluster cations, Cu$_n$O$_n^+$ ($n = 1-8$), and found that the clusters are planar up to $n = 3$.[22]

Most of the previous studies involved structural assignments based on theoretical calculations, and there have been few experimental studies on stable stoichiometric composition and geometric structures; even those were combined with theoretical calculations. In the present study, stoichiometric compositions and size-dependent structures of copper oxide cluster cations have been investigated by ion mobility mass spectrometry (IMMS).

IMMS, a combination of ion mobility spectrometry (IMS) and MS, is a useful analytical method to study the structures of

gas-phase ions.[23−25] In the conventional drift-tube-type IMS, an ion packet is injected into a gas cell (ion-drift cell) in which an electrostatic field is applied. Due to a mutual effect of acceleration of ions by the electrostatic field, $E$, and deceleration by collisions with buffer gas atoms in the cell, the drift velocity of the ions, $v_d$, becomes a constant proportional to $E$, i.e.,

$$v_d = KE \tag{1}$$

in which the coefficient $K$ is defined as ion mobility.[26]

The equation for the ion mobility $K$ of thermalized ions traveling through the buffer gas in the electrostatic field is given from the kinetic theory of ion transport as

$$K = \frac{3e}{16N} \sqrt{\frac{2\pi}{k_B \mu T_{eff}}} \frac{1}{\Omega} \tag{2}$$

where $e$ is the elementary charge, $N$ is the number density of the buffer gas atoms, $k_B$ is the Boltzmann constant, $\mu$ is the reduced mass of the ion and the buffer gas atom, and $\Omega$ is the collision integral, representing an average of momentum transfer cross sections over collision energies and orientations.[26] When we treat the ion and neutral parts as hard spheres without internal states, the collision integral can be reduced to the hard-sphere collision cross section (CCS). The term $T_{eff}$, the effective temperature of the ions, is given by $T_{BG} + M_B v_d^2 / 3k_B$, where $T_{BG}$ is the buffer gas temperature and $M_B$ is the mass of the buffer gas. Thus, the time that the ion spends in the ion-drift cell is inversely proportional to $K$ and directly proportional to $\Omega$, as derived from eqs 1 and 2.[27] Therefore, the CCS of the ion can be evaluated by measuring the ion mobility in the drift cell.

Recently, we studied the structures of metal oxide cluster ions of first-row transition metals, such as, Zn,[28] Co,[29] Fe,[30] Ni,[31] Ti,[32] V,[33] and Cr,[34] by IMMS. Transitions from two-dimensional (2D) to three-dimensional (3D) structures were commonly observed in the cluster ions of oxides of the metals of the latter half of this row.[28−31] In the present study, the structures of copper oxide cluster cations, $Cu_nO_m^+$, have been studied by IMMS. Experimental CCSs of these cluster ions were determined by measuring the ion mobility. In addition, theoretical CCSs were calculated by the MOBCAL program[35] for optimized structures obtained by theoretical calculations. By comparing CCSs experimentally measured by IMMS and theoretically calculated CCSs for optimized structures, we are able to assign geometrical structures of the cluster ions. We discuss the structures of two different metal-to-oxygen ratios because the copper oxide exists as two stable oxides—$Cu_2O$ and CuO—in the condensed phase. In the present study, CCSs and structures of stable compositions of $Cu_nO_m^+$ with $n:m \approx 2:1$ (building unit: $Cu_2O$) and other cluster series, like $Cu_nO_n^+$ with $n:m = 1:1$ (building unit: CuO) and $Cu_nO_{n-1}^+$ (comprising both $Cu_2O$ and CuO), are assigned up to $n = 8$. The obtained structures are discussed as a function of the cluster size, and these structures are compared with the previous results for copper oxide cluster ions.

## 2. EXPERIMENTAL METHODS

IMMS experiments were performed using a vacuum apparatus composed of a source of cluster ions, an ion-drift cell, and a reflectron-type time-of-flight (TOF) mass spectrometer. Copper oxide cluster cations, $Cu_nO_m^+$, were formed by a combination of laser vaporization of a copper rod and

supersonic expansion of 5% $O_2$/He mixture gas (stagnation pressure was 2 atm). Cluster ions were introduced to the ion-drift cell with injection energies, $E_{inj}$, of 50 and 250 eV by applying a pulsed electric field at a given time ($t = t_0$). The ion-drift cell with length $L = 100$ mm was filled with He buffer gas (0.80 Torr). The cell was kept at 180 K by cooling with liquid $N_2$. The electrostatic field in the cell was $E = 10$ V/cm. After running through the cell, at a later time after the ion-injection pulse, $t = t_0 + \Delta t$, the cluster ions were accelerated to ~1.8 keV by another pulsed electrostatic field in an acceleration region of the TOF mass spectrometer. We defined this delay time, $\Delta t$, as the "arrival time". We calculated the actual time that an ion spends in the cell (drift time, $t_d$) from the arrival time by solving the equations of motion of the cluster ion, as explained in the Supporting Information. Because $t_d$ depends on the CCS between the ion and the He atom, cluster ions with different CCSs arrive at the source region of the TOF mass spectrometer at different arrival times. The cluster ions in this region were then mass-analyzed by the reflectron-type TOF mass spectrometer. In the IMMS measurement, we obtained TOF mass spectra sequentially by scanning the arrival times. As a result, cluster ions with different CCSs were detected separately at different arrival times in a 2D plot of TOF versus arrival time. We compiled an arrival time distribution (ATD) of cluster ions, in which the total ion intensity of a certain TOF peak is shown as a function of arrival time.

The ratio of the drift electrostatic field, $E$, to the number density of buffer gas atoms, $N$, is an important parameter in ion mobility measurements. The $E/N$ values were, in general, kept low, at 1.5–10 Td (1 Td (Townsend unit) = $10^{-17}$ V·cm²).[36,37] It is necessary to keep $E/N$ low in the measurement of reliable CCSs of cluster ions in the low-field limit ($E/N \to 0$ Td) because the mobility of ions in high $E/N$ conditions deviates from the data in the low field. However, the cluster-ion concentration decreases at low $E/N$ conditions because of scattering attributed to lots of collisions with the buffer gas. Thus, we optimized the highest possible $E/N$ conditions for determining the structures of cluster ions. The $E/N$ conditions were kept at 23 Td in the present measurement by setting buffer-gas pressure and temperature in the ion-drift cell at 0.80 Torr and 180 K, respectively. Under these conditions, the effective temperature of the $Cu_4O_2^+$ ion, for example, was estimated to be about 240 K. These conditions have already been confirmed as reliable to measure precise CCSs of ions by the author's group.[38]

## 3. COMPUTATIONAL METHODS

Density functional theory calculations for optimization of the structures of copper oxide cluster ions, $Cu_nO_m^+$, were performed prior to the calculations of the CCSs of the cluster ions. The optimizations were carried out by using the B3LYP/cc-pVDZ level in Gaussian 09.[39] We used singlet and doublet as spin multiplicities for even and odd numbers of copper atoms, respectively. The calculated relative energy ($\Delta E$) of each isomeric structure was also taken under consideration to find the relative stability of optimized structures. Theoretical CCSs, $\Omega_{calc}$, for those optimized structures were next calculated by using the MOBCAL[35] program. The collision integral of an ion with a He atom was calculated by the trajectory method (TM) which is included in the program. In the TM calculation of copper oxide cluster ions, the interaction potential between a $Cu_nO_m^+$ cluster ion and a He atom was

needed to calculate the CCSs. This interaction potential was represented by the sum of interaction potentials between constituent atoms (Cu and O atoms) and a He atom, $V_i^{Cu-He}(r_i)$ and $V_i^{O-He}(r_i)$, as shown in eq 3,

$$V_i^{X-He}(r_i) = 4\varepsilon^{X-He}\left[\left(\frac{\sigma^{X-He}}{r_i}\right)^{12} - \left(\frac{\sigma^{X-He}}{r_i}\right)^6\right] - \frac{\alpha e^2}{2}\frac{q_i^2}{r_i^4}$$

$$(X = Cu, O) \tag{3}$$

where $r_i$ is the distance between the $i$th constituent atom and a He atom, $\varepsilon^{X-He}$ and $\sigma^{X-He}$ are the Lennard-Jones parameters, $\alpha$ is the polarizability of a He atom, and $q_i$ is the atomic charge on the $i$th atom. In the present calculations, we used the $\varepsilon^{X-He}$ values which were reported previously from theoretical calculations ($\varepsilon^{Cu-He}$ = 0.773 meV and $\varepsilon^{O-He}$ = 2.596 meV).[40,41] For $\sigma^{X-He}$, we used the sum of van der Waals radii of Cu or O atoms (2.00 or 1.52 Å) with He (1.40 Å) ($\sigma^{Cu-He}$ = 3.40 Å and $\sigma^{O-He}$ = 2.92 Å).[42,43] Atomic charges calculated by natural population analysis were used for $q_i$. The temperature was 180 K in the calculations. The uncertainty of the calculated CCS was about 1 Å$^2$ when the CCS value was 50 Å$^2$. In eq 3 of ref 35, $\sigma$ is defined as the distance ($r_0$) where the potential becomes positive. However, when we used the distance $r_0$ in CCS calculations, CCSs were calculated 6−10 Å$^2$ larger than CCSs in the present study. Because it was impossible to assign structures of cluster ions with these large CCSs, we used the sum of van der Waals radii instead of $r_0$ in the present CCS calculations.

## 4. RESULTS AND DISCUSSION

**4.1. Mass Spectra of Cluster Cations.** Stoichiometric compositions are discussed in this section, based on the mass spectra obtained in the IMMS measurement, as shown in Figure 1, mainly from the injection energy dependence of the
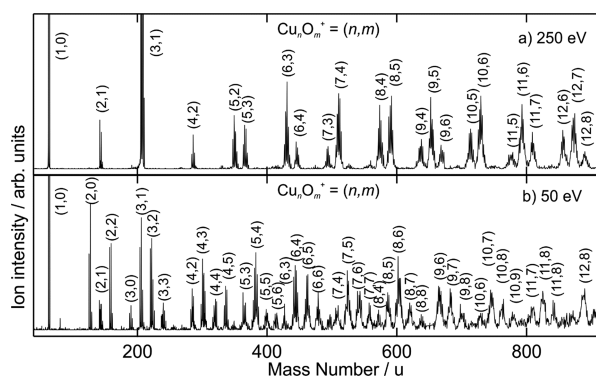


**Figure 1.** Typical mass spectra of copper oxide cluster cations after collisions with buffer gas atoms in the ion-drift cell. Ion-injection energies ($E_{inj}$) were (a) 250 and (b) 50 eV. The pressure of the buffer gas and temperature of the ion-drift cell were 0.80 Torr and 180 K, respectively.

cluster ions moving into the ion-drift cell. Some metal oxide cluster ions have tendencies to be populated to specific compositions with increasing injection energy because of CID just after their injection into the ion-drift cell before thermalization. In the present apparatus, TOF mass spectra of copper oxide cluster cations were obtained by summing all the ion signals at every arrival time existing in the ion-drift cell with spatial distributions depending on their mobilities.

At the 250 eV injection energy condition for the mass spectra shown in Figure 1a, oxygen-deficient clusters of $Cu_nO_m^+$ showed intense signals up to $n$ = 12. More specifically, $Cu^+$, $Cu_2O^+$, $Cu_3O^+$, $Cu_4O_2^+$, $Cu_5O_m^+$ ($m$ = 2, 3), $Cu_6O_m^+$ ($m$ = 3, 4), $Cu_7O_m^+$ ($m$ = 3, 4), $Cu_8O_m^+$ ($m$ = 4, 5), $Cu_9O_m^+$ ($m$ = 4−6), $Cu_{10}O_m^+$ ($m$ = 5, 6), $Cu_{11}O_m^+$ ($m$ = 6, 7), and $Cu_{12}O_m^+$ ($m$ = 6−8) were observed in the TOF mass spectrum. We hereafter denote the $Cu_nO_m^+$ ion as ($n, m$) in the figures. These ions can be classified as $(Cu_2O)_{n/2}^+$ ($n$ = 2, 4, 6, 8, 10, and 12), $Cu_nO_{(n-1)/2}^+$ ($n$ = 3, 5, 7, 9, and 11), and $Cu_nO_{(n+1)/2}^+$ ($n$ = 5, 7, 9, and 11). Except for some large cluster ions with more oxygens such as ($n, m$) = (9, 6), (11, 7), the ion species observed at this injection energy show metal-to-oxygen ratios of ∼ 2:1.

In addition to the mass spectra obtained at 250 eV injection energy, the mass spectra at the lower injection energy of 50 eV are shown in Figure 1b. At this energy, a variety of cluster species were observed in the mass spectrum than were not seen in that taken at 250 eV. Such cluster species can be classified into several series, for example, oxygen-rich ions, $Cu_nO_{n+1}^+$ ($n$ = 4, 5), and oxygen-equivalent ions, $Cu_nO_n^+$ ($n$ = 2−8). Oxygen-deficient ions were also observed in the mass spectrum, such as $Cu_nO_{n-1}^+$ ($n$ = 2−10), $(Cu_2O)_{n/2}^+$ ($n$ = 2−8 with $n$ even), and $Cu_nO_{(n+1)/2}^+$ ($n$ = 3−11 with $n$ odd). Some of the oxygen-deficient species found in both mass spectra, at the 250 and 50 eV injection energies, e.g., $Cu_2O^+$, $Cu_3O^+$, $Cu_4O_2^+$, $Cu_5O_{2-3}^+$, $Cu_6O_{3-4}^+$, $Cu_7O_4^+$, and $Cu_8O_{4-5}^+$, were also observed in mass spectra of cluster ions generated by laser ablation/ionization in the previous studies.[14−17]

As noted above, the cluster ions observed at 250 eV injection energy can, in general, be regarded as relatively stable species among copper oxide cluster ions with respect to CID. As a result of CID processes, oxygen-rich and oxygen-equivalent clusters have a tendency to prefer to be dissociated to a variety of oxygen-deficient cluster series, like $(Cu_2O)_{n/2}^+$ ($n$ even), $Cu_nO_{(n-1)/2}^+$ ($n$ odd), and $Cu_nO_{(n+1)/2}^+$ ($n$ odd), by the loss of oxygen atoms. These results of CID have been also observed by Hirabayashi and Ichihashi.[44] Moreover, the relative intensities of the small stable species were found to be higher under high injection energy because of the fragmentation of larger cluster ions.

**4.2. 2D Plot of Time-of-Flight (TOF) versus Arrival Time and Arrival Time Distributions (ATDs).** A 2D-plot of TOF vs arrival time for copper oxide cluster cations, $Cu_nO_m^+$, at the ion-injection energy of 50 eV is shown in Figure 2. In this plot, the horizontal axis is TOF, corresponding to the mass number, and the vertical axis is the arrival time, which is almost proportional to the CCS of each cluster ion. Due to the weak ion intensity for larger cluster ions observed with the present instrument, the 2D plot up to $n$ = 8 is shown in the figure. The
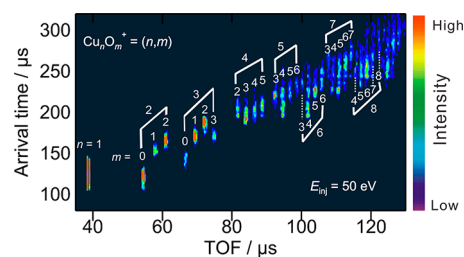


**Figure 2.** 2D plot for copper oxide cluster cations at the ion-injection energy of 50 eV.
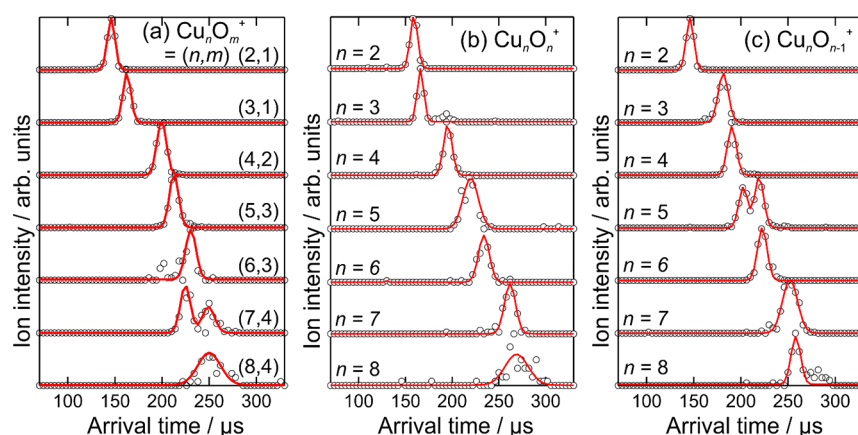
**Figure 3.** Arrival time distributions of (a) $Cu_nO_{\sim n/2}{}^+$ and $Cu_3O^+$, (b) $Cu_nO_n{}^+$, and (c) $Cu_nO_{n-1}{}^+$ for $n = 2-8$, measured at the ion-injection energy of 50 eV. Red solid curves are Gaussian functions which were used for fitting the experimental plots (black circles).

arrival time of an ion has, in general, an increasing tendency with the mass of the ion because of the increase of the number of the constituent atoms. However, in this 2D spectrum, the arrival time of some ions did not increase monotonically with the mass of the cluster ion. In particular, the arrival times of $Cu_3O_3{}^+$ and $Cu_4O_3{}^+$ were shorter than those of their prior neighboring compositions, $Cu_3O_2{}^+$ and $Cu_4O_2{}^+$, respectively. This feature indicates that the former ions might have more compact geometries than the latter ions. In order to deduce the experimental CCSs ($\Omega_{exp}$) of the cluster ions, ATDs were first determined from this 2D plot. The peak values of the arrival times were determined by fitting the ATDs with Gaussian functions, as shown in Figure 3. In order to estimate reliable $\Omega_{exp}$ values, ATDs were analyzed for the data measured under the low injection energy condition ($E_{inj}$ = 50 eV). This is because the high $E_{inj}$ condition not only causes CID, resulting in stable species, but also causes a longer deceleration time for the cluster ion until the cluster reaches a constant drift velocity ($v_d$). As a result, the injected ions tend to have shorter arrival times, and thus the high $E_{inj}$ condition results in underestimated CCSs. The CCSs and structures of stable compositions such as $Cu_nO_m{}^+$ $n:m \approx 2:1$ and the $Cu_3O^+$ ion, which were observed at both 250 and 50 eV, are discussed in section 4.3.1. Some other compositions which contained more oxygen, such as $Cu_nO_n{}^+$ and $Cu_nO_{n-1}{}^+$, were also selected for CCS calculations and structural determination, discussed separately in section 4.3.2.

**4.3. Structural Assignment by Comparison of Experimental and Theoretical Results.** *4.3.1. Structural Assignments of the Most Abundant Compositions, $Cu_nO_{\sim n/2}{}^+$.* As shown in Figure 3a, where narrow ATD profiles were fitted well by only one Gaussian function and changed gradually, the most stable species, $(Cu_2O)_{\sim n/2}{}^+$ and $Cu_3O^+$, were suggested to have one structural isomer or a family of structures with close CCSs. However, the ATD of $Cu_7O_4{}^+$ was considerably broader and showed two separate peaks, and thus two Gaussian functions were necessary for fitting the ATD of this cluster ion. This observation suggested that two structural isomers with different CCSs might coexist for $Cu_7O_4{}^+$.

Calculated structures are shown in Figure 4 for cluster cations with the compositions $Cu_2O^+$, $Cu_3O^+$, $Cu_4O_2{}^+$, $Cu_5O_3{}^+$, $Cu_6O_3{}^+$, $Cu_7O_4{}^+$, and $Cu_8O_4{}^+$, which were observed most abundantly in Figure 1. The experimental CCS, $\Omega_{exp}$, of each composition is also shown in the same figure, along with the theoretical CCSs, $\Omega_{calc}$, of the structures optimized in the



**Figure 4.** Schematic representation and assigned structures for stable cluster cations of $Cu_2O^+$, $Cu_3O^+$, $Cu_4O_2{}^+$, $Cu_5O_3{}^+$, $Cu_6O_3{}^+$, $Cu_7O_4{}^+$, and $Cu_8O_4{}^+$. Calculated CCSs ($\Omega_{calc}/Å^2$) and relative energies from the most stable isomers ($\Delta E/eV$, in parentheses) are also shown with experimental CCSs ($\Omega_{exp}/Å^2$).

DFT calculations. Calculated isomers not presented in this figure are shown in the Supporting Information (Figure S1). The experimental CCS was determined from the ATD with an error of one standard deviation of the data for five independent measurements.

As shown in Figure 4 for $Cu_2O^+$, the most stable structure with a bent geometry has a theoretical CCS which is in good agreement with the experimental CCS. This structure is almost the same as that reported previously.[20] In the $Cu_3O^+$ cluster, the most stable structure has a triangle geometry in which three copper atoms are attached to the central oxygen atom. This structure also can be made simply by adding one copper atom to the bridging oxygen of the $Cu_2O^+$ geometry noted above. This triangular planar structure is supported by comparison of the CCS values between experiment (50.9 ±

$Cu_nO_n^+$



**Figure 5.** Optimized structural candidates for $Cu_nO_n^+$ for $n = 2-8$, calculated at the B3LYP/cc-pVDZ level. The corresponding theoretical CCSs ($\Omega_{calc}/\text{Å}^2$) and relative energies for the most stable structure ($\Delta E/eV$, in parentheses) are shown below the structures. For comparison, the experimental CCSs ($\Omega_{exp}/\text{Å}^2$) are also labeled along with standard deviations. The structures with the theoretical CCS closest to the experimental value are shown as the best-fitted structures. Other possible structures are indicated by underlines from the comparison between $\Omega_{exp}$ and $\Omega_{calc}$.

2.5 Å$^2$) and theory (50.4 Å$^2$), and it is also supported by the previous theoretical study.[45] The most stable structure of $Cu_4O_2^+$ was concluded to be a 2D branched one, as shown in Figure 4, which was already reported theoretically.[20] Again, this structure of $Cu_4O_2^+$ can be formed by aggregation of triangular $Cu_3O^+$ and a CuO unit: the CuO unit, attached from the oxygen side with one of the Cu ends of the $Cu_3O^+$ cluster ion, gives a branched 2D geometry for the $Cu_4O_2^+$ cluster cation. This structure was assigned for $Cu_4O_2^+$ also from the CCS comparison: the $\Omega_{calc}$ value of the branched 2D geometry (65.8 Å$^2$) showed good agreement with the $\Omega_{exp}$ (64.4 ± 2.8 Å$^2$) within the standard deviation. For the $Cu_5O_3^+$ cluster ion, the 2D closed-ring geometry, which is the most stable structure in the calculations shown in Figure 4, was assigned as plausible since $\Omega_{calc}$ of this symmetrical closed-ring structure, 71.3 Å$^2$, was close to $\Omega_{exp}$ (69.0 ± 3.4 Å$^2$). This structure can be constructed by adding one CuO unit to the branched 2D $Cu_4O_2^+$ geometry: the oxygen atom was bonded to the bicoordinated bridged oxygen and copper atoms bonded to the terminal oxygen of $Cu_4O_2^+$, consequently forming the closed-ring 2D structure. For the $Cu_6O_3^+$ cluster ion, adding a Cu unit to the aforementioned $Cu_5O_3^+$ cluster geometry also yields a similar closed-ring 2D geometry. This time, an extra Cu atom coordinated with the doubly bonded O atom of the $Cu_5O_3^+$ geometry. This structure was also assigned to be the most probable because the theoretical CCS of the structure, 78.3 Å$^2$, was close to the CCS obtained in the IMMS measurement, 77.3 ± 1.4 Å$^2$. For $Cu_7O_4^+$ and $Cu_8O_4^+$, the systematic growth of structures noted above for the small clusters appeared to be terminated on the basis of the experimental results, as shown in Figure 3a. Additionally, two structural isomers were assigned for $Cu_7O_4^+$ in the ATD distribution: one a symmetrical 2D

geometry with a longer arrival time and the other a compact 3D geometry with a shorter arrival time. The latter isomer has an arrival time shorter than that for $Cu_6O_3^+$. Also, for the $Cu_8O_4^+$ cluster ion, a compact 3D structure was assigned by comparison between the experimental and calculated CSSs. Relatively lower increments were observed in the arrival time with increasing $n$ at $n = 7$ and 8 than those in the composition with smaller $n$ (Figure 3a).

*4.3.2. Structural Assignments of the $Cu_nO_n^+$ and $Cu_nO_{n-1}^+$ Series.* In this section, the structural assignment concentrated on the cluster ions containing more oxygen atoms, which were mostly observed at the 50 eV injection energy condition. As mentioned in section 4.2, ATDs were obtained for the $Cu_nO_n^+$ and $Cu_nO_{n-1}^+$ series, as shown in Figure 3b,c. The ATDs of the $Cu_nO_n^+$ ($n = 2-8$) cluster cations shown in Figure 3b had narrow profiles and were fitted well with one Gaussian function, which indicated the presence of one structural isomer or a family of multiple structures with close CCSs. The ATDs of this series did not changed smoothly with cluster size but changed rather unevenly. Specifically, the arrival time of $Cu_3O_3^+$ is almost the same as that of $Cu_2O_2^+$. The increments in the arrival times between $Cu_5O_5^+$ and $Cu_6O_6^+$ and those between $Cu_7O_7^+$ and $Cu_8O_8^+$ were also smaller than in the other cases. These differences in trends in consecutive ATD plots might reflect details about the growth of the geometrical structures.

In the oxygen-deficient $Cu_nO_{n-1}^+$ series ($n = 2-8$) shown in Figure 3c, the ATD plots were also all fitted by only one Gaussian function, except for $Cu_5O_4^+$. Similar to the $Cu_7O_4^+$ cluster ion mentioned in section 4.3.1, the $Cu_5O_4^+$ cluster ion was also predicted to have two structural isomers with different CCSs. Meanwhile, stepwise growth of ATDs at some cluster

$Cu_nO_{n-1}{}^+$

| n $\Omega_{exp}$ (Å²) | best-fitted structures | | other candidates | | | | |
|---|---|---|---|---|---|---|---|
| | 2D | 3D | 1D | 2D | 2D | 3D | 3D |
| 2 45.1±2.8 | $\Omega_{calc}$= 44.5 ΔE = 0.0 eV | | 44.2 (1.35) | | | | ●···Cu ●···O |
| 3 58.3±2.7 | 58.3 (0.00) | | 58.4 (0.01) | 54.5 (0.39) | | 55.4 (0.44) | 51.9 (0.06) |
| 4 60.1±2.5 | | 60.1 (0.19) | 72.5 (1.26) | 65.3 (0.00) | 65.2 (0.39) | 73.4 (1.52) | 60.9 (0.15) |
| 5 63.0±2.6 70.9±3.3 | 69.1 (0.00) | 64.9 (1.00) | | 75.2 (0.72) | | 78.64 (1.56) | 68.2 (1.92) |
| 6 71.5±3.1 | | 74.2 (0.42) | | 91.5 (0.74) | 76.9 (0.91) | 82.3 (1.30) | 75.6 (0.00) |
| 7 84.0±4.1 | | 84.7 (0.00) | | 101.9 (0.81) | 87.9 (0.56) | 83.1 (0.54) | 78.8 (0.46) |
| 8 85.7±4.3 | | 88.5 (0.01) | | 96.3 (0.58) | | 89.5 (1.08) | 89.2 (0.00) |

**Figure 6.** Optimized structural candidates for $Cu_nO_{n-1}{}^+$ for n = 2−8, calculated at the B3LYP/cc-pVDZ level. The corresponding theoretical CCSs ($\Omega_{calc}$/Å²) and relative energies for the most stable structure (ΔE/eV, in parentheses) are shown below the structures. For comparison, the experimental CCSs ($\Omega_{exp}$/Å²) are also labeled along with standard deviations. The structures with the theoretical CCS closest to the experimental value are shown as the best-fitted structures. Other possible structures are indicated by underlines from the comparison between $\Omega_{exp}$ and $\Omega_{calc}$.

size was observed for the whole $Cu_nO_{n-1}{}^+$ series. For example, the arrival times of $Cu_3O_2{}^+$ and $Cu_4O_3{}^+$ were almost the same. Similarly, the ATDs obtained for the slower components of $Cu_5O_4{}^+$ and $Cu_6O_5{}^+$, and also for $Cu_7O_6{}^+$ and $Cu_8O_7{}^+$, were almost the same. These results indicate stepwise structural growth at these cluster sizes, and, importantly, they imply that the later species might contain comparatively compact structures.

Structural candidates along with their experimental CCSs ($\Omega_{exp}$/Å²), theoretical CCSs ($\Omega_{calc}$/Å²), and relative energies ($\Delta E$/eV) for $Cu_nO_n{}^+$ and $Cu_nO_{n-1}{}^+$ are summarized in Figures 5 and 6. These structural candidates were classified into best-fitted structures and other candidate structures. The structures with theoretical CCSs close to the experimental CCSs were considered as best-fitted structures.

As shown in Figure 5, the most stable ($\Delta E = 0$) structures of n = 2−8 were either 2D (n = 2, 3, and 6) or 3D structures (n = 4, 5, 7, and 8) for $Cu_nO_n{}^+$ cations. This stability trend is somewhat different from the IMS results of the other oxide cluster ions of 3d transition metals, Fe, Co, Ni, and Zn, reported previously by the authors' group.[28−31] For example, stable structures of $M_nO_n{}^+$, with M = Fe, Ni, Co, and Zn, were predicted as either ring or cubic for n = 4 and 5. However, the most stable structures for $Cu_4O_4{}^+$ and $Cu_5O_5{}^+$ were found to be 3D structures containing an O−O bond, which were also previously obtained theoretically by another group.[22] For $Cu_2O_2{}^+$, $\Omega_{calc}$ of the 2D zigzag planar isomer (49.9 Å²) was found to be in good agreement with $\Omega_{exp}$ (50.2 ± 2.5 Å²). As for $Cu_3O_3{}^+$, $\Omega_{calc}$ of the best-fitted structure (56.3 Å²) or the most stable cyclic structure (56.9 Å²) did not agree well with $\Omega_{exp}$ (51.4 ± 2.3 Å²) at the present calculation level. In fact, the 2D plot of arrival time vs TOF, shown in Figure 2, revealed

that the arrival time for $Cu_3O_3{}^+$ fell abruptly compared with that of the prior-size neighbor. Therefore, a more compact structure was suggested for the $Cu_3O_3{}^+$ cluster. This tendency was also observed in Figure 7, where the theoretical CCS, $\Omega_{calc}$, of this structure shows the same trend with the experimental CCS, $\Omega_{exp}$.
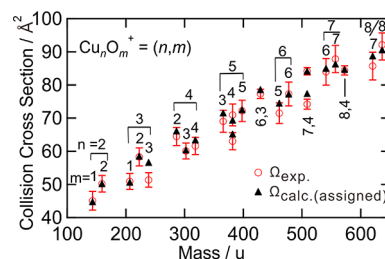


**Figure 7.** Experimental collision cross sections obtained by ion mobility experiments, $\Omega_{exp}$, for copper oxide cluster cations, $Cu_nO_m{}^+$, plotted as red circles. Theoretical cross sections, $\Omega_{calc}$, for the assigned structures are plotted as black triangles.

For $Cu_4O_4{}^+$, $\Omega_{calc}$ of the O−O bonded nonplanar isomer (65.3 Å²), which was the most stable, was a little larger than $\Omega_{exp}$ (61.6 ± 2.6 Å²), while $\Omega_{calc}$ of the 3D box structure (63.1 Å²) was closer to $\Omega_{exp}$. Therefore, the 3D compact structure was suggested for $Cu_4O_4{}^+$. For $(CuO)_{5-8}{}^+$, we obtained 3D-type isomers which have comparable $\Omega_{calc}$ and $\Omega_{exp}$ values, although they were less stable, especially for $Cu_5O_5{}^+$ and $Cu_6O_6{}^+$. For $Cu_5O_5{}^+$, three candidate structures (CCSs underlined) shown in Figure 5 have 3D structures which grow from or slightly distorted from 2D isomers. For $Cu_6O_6{}^+$, $\Omega_{calc}$ of the 3D compact structure (77.0 Å²) was in good

agreement with $\Omega_{exp}$ (77.3 ± 3.7 Å$^2$), whereas the most stable isomer has a 2D sheet-like structure. Both the 2D sheet (90.6 Å$^2$) and the 3D compact (86.0 Å$^2$) isomers were assigned for the structures of $Cu_7O_7^+$ because they have CCSs comparable with $\Omega_{exp}$ (87.8 ± 4.2 Å$^2$). A tendency similar to that seen with the $Cu_6O_6^+$ ion was observed for $n = 8$: the 3D isomers were assigned as the most probable structures for the $Cu_8O_8^+$ cluster ion. The experimental CCS difference from $n = 4$ ($\Omega_{exp} = 61.6$ Å$^2$) to $n = 5$ ($\Omega_{exp} = 72.2$ Å$^2$) is 10.6 Å$^2$, while the CCS difference from $n = 5$ ($\Omega_{exp} = 72.2$ Å$^2$) to $n = 6$ ($\Omega_{exp} = 77.3$ Å$^2$) is only 5.1 Å$^2$, which is almost half that of the prior compositions. The same phenomenon was noted for $n = 6$ ($\Omega_{exp} = 77.3$ Å$^2$) to $n = 7$ ($\Omega_{exp} = 87.8$ Å$^2$), and from $n = 7$ ($\Omega_{exp} = 87.8$ Å$^2$) to $n = 8$ ($\Omega_{exp} = 92.1$ Å$^2$), where CCS differences are 10.5 and 4.3 Å$^2$, respectively. This observation of large CCS differences from $n = 4$ to 5 and from $n = 6$ to 7 was explained by the existence of 2D structures at $n = 5$ and 7 in addition to 3D isomers.

From the structural candidates of $Cu_nO_{n-1}^+$ series shown in Figure 6, 2D structures were found to be the most stable ($\Delta E = 0$) structures for $n = 2$–5 and 3D structures for $n = 6$–8 at the present calculation level. The structure of $Cu_2O^+$ was assigned in section 4.3.1. For $Cu_3O_2^+$, two types of 2D structures, the most stable zigzag and another bent isomer with slightly higher energy, were assigned in this study: the $\Omega_{calc}$ values of the zigzag (58.3 Å$^2$) and 2D bent (58.4 Å$^2$) isomers were in good agreement with $\Omega_{exp}$ (58.3 ± 2.7 Å$^2$). Because the experimental CCSs for $Cu_3O_2^+$ and $Cu_4O_3^+$ were found to be very close, as it was suggested from ATDs in Figure 3c, the $Cu_4O_3^+$ ion should have a structure different from the 2D structure, like $Cu_3O_2^+$. Although a 2D cyclic isomer was found to be the most stable in the present calculation, its theoretical CCS (65.3 Å$^2$) was much larger than the experimental value (60.1 ± 2.5 Å$^2$). Instead, two 3D compact structures for the $Cu_4O_3^+$ cluster ion were assigned as probable structures, because they have theoretical $\Omega_{calc}$ (60.9 and 60.1 Å$^2$) similar to $\Omega_{exp}$, and also because they have very little energy differences ($\Delta E = 0.15$ and 0.19 eV, respectively) from the most stable structure. As observed in Figure 3c, two Gaussian functions were fitted to the ATD of the $Cu_5O_4^+$ cluster ion, indicating the coexistence of at least two different structural isomers. From the calculations, $\Omega_{calc}$ of the 3D compact isomer (64.9 Å$^2$) of $Cu_5O_4^+$ cluster ion was found to be the closest to the smaller $\Omega_{exp}$ (63.0 ± 2.6 Å$^2$), whereas $\Omega_{calc}$ of a 2D sheet structure (69.1 Å$^2$; $\Delta E = 0$ eV) was in agreement with larger $\Omega_{exp}$ (71.0 ± 2.6 Å$^2$). Therefore, it can be concluded that the 2D sheet and the 3D compact structures coexist in $Cu_5O_4^+$. Moreover, the observation that the CCSs of the larger isomer of $Cu_5O_4^+$ and $Cu_6O_5^+$ are almost equal indicates that the $Cu_6O_5^+$ ion should have more compact structures than the 2D sheet isomer of $Cu_5O_4^+$. $\Omega_{calc}$ of the most stable 3D isomer (75.6 Å$^2$; $\Delta E = 0$ eV) of $Cu_6O_5^+$ was found to be a little larger than $\Omega_{exp}$ (71.5 ± 3.1 Å$^2$), and $\Omega_{calc}$ for the other 3D compact structure (74.2 Å$^2$; $\Delta E = 0.4$ eV) was in good agreement with $\Omega_{exp}$ within the standard deviation limit. Therefore, the latter 3D compact structure was assigned as the most plausible structure for $Cu_6O_5^+$. For the $Cu_7O_6^+$ ion, two 3D isomers ($\Omega_{calc} = 84.7$ Å$^2$; $\Delta E = 0$ eV, and $\Omega_{calc} = 83.1$ Å$^2$; $\Delta E = 0.5$ eV) and a sheet-type 2D isomer ($\Omega_{calc} = 87.9$ Å$^2$; $\Delta E = 0.6$ eV) were found to have CCSs comparable with $\Omega_{exp}$ (85.7 ± 4.3 Å$^2$). Hence, these 2D sheet and 3D compact structures were assigned as structural candidates for the $Cu_7O_6^+$ cluster cation. Similar to the previous pair of $Cu_5O_4^+$ and $Cu_6O_5^+$, the

observed ATD band position of $Cu_8O_7^+$ was almost same as that of its preceding neighbor, $Cu_7O_6^+$, as shown in Figure 3c. The $\Omega_{calc}$ values of a few 3D isomers were comparable but a little larger than $\Omega_{exp}$ for $Cu_8O_7^+$. Therefore, such 3D structures were tentatively assigned as structural candidates for $Cu_8O_7^+$.

## 5. CONCLUSION

Stable compositions and structures of copper oxide cluster cations were assigned in this study on the basis of a comparison of collision cross sections (CCSs) obtained in experiments and in theory. This target was achieved experimentally with ion mobility mass spectrometry and theoretically with theoretical calculations. In this study, mass spectra of copper oxide cluster cations ($Cu_nO_m^+$) were measured at two different injection energies of 250 and 50 eV into the ion-drift cell for ion mobility measurement. Stable compositions were obtained with respect to collision-induced dissociation just inside of the ion-drift cell from this experiment, and they were assigned as $Cu_nO_m^+$, $n{:}m \approx 2{:}1$. In the present study, it was mainly these stable compositions that were analyzed for structural assignment. Other important cluster series, $Cu_nO_n^+$ and $Cu_nO_{n-1}^+$ ($n = 2$–8), which were observed only at 50 eV injection energy condition, were also analyzed to assign the structures. Arrival time distributions (ATDs) of these ion series were obtained from the 2D plot of copper oxide cluster cations. Experimental CCSs were deduced from ATDs. Theoretical CCSs were calculated for stable structures optimized by quantum chemical calculations. The structures of copper oxide cluster cations were determined by comparison between experimental and theoretical CCSs. Systematic structural growth was observed for the stable compositions of $Cu_nO_m^+$, $n{:}m \approx 2{:}1$, up to $n = 6$, and then complex shapes began to appear for $n = 7$ and 8. Both 2D and 3D compact structures were assigned for $Cu_nO_n^+$. In the case of the $Cu_nO_{n-1}^+$ cluster ion, stepwise structural growth was observed from 2D to 3D for sizes $Cu_3O_2^+$ to $Cu_4O_3^+$, $Cu_5O_4^+$ to $Cu_6O_5^+$, and $Cu_7O_6^+$ to $Cu_8O_7^+$. Additionally, 2D sheet and 3D compact isomers were found to coexist in the $Cu_5O_4^+$ and $Cu_7O_4^+$ cluster ions.

## ■ ASSOCIATED CONTENT

**ⓢ Supporting Information**

The Supporting Information is available free of charge on the ACS Publications website at DOI: 10.1021/acsomega.8b02466.

> All calculated isomers optimized at the B3LYP/cc-pVDZ level in Gaussian 09 for the most abundant (stable) compositions, reduced ion mobility, details of the method for estimating drift time and drift velocity, and Cartesian coordinates and natural charges of all assigned geometries (PDF)

## ■ AUTHOR INFORMATION

**Corresponding Author**

*Tel.: +81 22 795 6577. Fax: +81 22 795 6580. E-mail: misaizu@m.tohoku.ac.jp.

**ORCID** ⓘ

Motoyoshi Nakano: 0000-0002-9615-2206
Keijiro Ohshimo: 0000-0002-2397-6896
Fuminori Misaizu: 0000-0003-0822-6285

## Notes

The authors declare no competing financial interest.

## REFERENCES

(1) Fisher, I. A.; Bell, A. T. In Situ Infrared Study of Methanol Synthesis from $H_2$/CO over $Cu/SiO_2$ and $Cu/ZrO_2/SiO_2$. *J. Catal.* **1998**, *178*, 153−173.

(2) Köppel, R. A.; Stöcker, C.; Baiker, A. Copper- and Silver-Zirconia Aerogels: Preparation, Structural Properties and Catalytic Behavior in Methanol Synthesis from Carbon Dioxide. *J. Catal.* **1998**, *179*, 515−527.

(3) Reitz, J. B.; Solomon, E. I. Propylene Oxidation on Copper Oxide Surfaces: Electronic and Geometric Contributions to Reactivity and Selectivity. *J. Am. Chem. Soc.* **1998**, *120*, 11467−11478.

(4) Huang, Y.-J.; Wang, H. P. Reduction of NO with $CH_4$ Effected by Copper Oxide Clusters in the Channels of ZSM-5. *J. Phys. Chem. A* **1999**, *103*, 6514−6516.

(5) Chi, Y.; Chuang, S. S. C. Infrared Study of NO Adsorption and Reduction with C3H6 in the Presence of $O_2$ over $CuO/Al_2O_3$. *J. Catal.* **2000**, *190*, 75−91.

(6) Jeong, S. S.; Mittiga, A.; Salza, E.; Masci, A.; Passerini, S. Electrodeposited $ZnO/Cu_2O$ heterojunction solar cells. *Electrochim. Acta* **2008**, *53*, 2226−2231.

(7) Siripala, W.; Ivanovskaya, A.; Jaramillo, T. F.; Baeck, S.-H.; McFarland, E. W. A $Cu_2O/TiO_2$ heterojunction thin film cathode for photoelectrocatalysis. *Sol. Energy Mater. Sol. Cells* **2003**, *77*, 229−237.

(8) Yu, Y.; Du, F.-P.; Yu, J. C.; Zhuang, Y.-Y.; Wong, P.-K. One-dimensional shape-controlled preparation of porous $Cu_2O$ nano-whiskers by using CTAB as a template. *J. Solid State Chem.* **2004**, *177*, 4640−4647.

(9) Razali, N. A. M.; Lee, K. T.; Bhatia, S.; Mohamed, A. R. Heterogeneous catalysts for production of chemicals using carbon dioxide as raw material: A review. *Renewable Sustainable Energy Rev.* **2012**, *16*, 4951−4964.

(10) Ma, L. L.; Li, J. L.; Sun, H. Z.; Wang, J. B.; Yu, Y.; et al. Self-assembled $Cu_2O$ flowerlike architecture: Polyol synthesis, photo-catalytic activity and stability under simulated solar light. *Mater. Res. Bull.* **2010**, *45*, 961−968.

(11) Luo, Y.; Li, S.; Ren, Q.; Liu, J.; Xing, L.; Wang, Y.; Yu, Y.; Jia, Z.; Li, J. Facile Synthesis of Flowerlike $Cu_2O$ Nanoarchitectures by a Solution Phase Route. *Cryst. Growth Des.* **2007**, *7*, 87−92.

(12) Minami, T.; Miyata, T.; Ihara, K.; Minamino, Y.; Tsukada, S. Effect of ZnO film deposition methods on the photovoltaic properties of $ZnO-Cu_2O$ heterojunction devices. *Thin Solid Films* **2006**, *494*, 47−52.

(13) Mittiga, A.; Salza, E.; Sarto, F.; Tucci, M.; Vasanthi, R. Heterojunction solar cell with 2% efficiency based on a $Cu_2O$ substrate. *Appl. Phys. Lett.* **2006**, *88*, 163502.

(14) Gord, J. R.; Bemish, R. J.; Freiser, B. S. Collision-induced dissociation of positive and megative copper oxide cluster ions generated by direct laser desorption/ionization of copper oxide. *Int. J. Mass Spectrom. Ion Processes* **1990**, *102*, 115−132.

(15) Aubriet, F.; Poleunis, C.; Chaoui, N.; Maunit, B.; Millon, E.; Muller, J. F.; Bertrand, P. Laser ablation and static secondary ion mass spectrometry capabilities in the characterization of inorganic materials. *Appl. Surf. Sci.* **2002**, *186*, 315−321.

(16) Ma, C. S.; Li, H. Y.; Zhang, X. G.; Bai, J. L.; Wang, X. Y.; Wang, L.; Zhang, G. Q.; He, G. Z.; Lou, N. Q. Formation of copper oxide cluster ions − Copper oxide cluster ions generated by direct laser ablation of copper oxide solid. *Prog. Nat. Sci.* **1996**, *6*, 159−164.

(17) Morita, K.; Sakuma, K.; Miyajima, K.; Mafuné, F. Thermally and Chemically Stable Mixed Valence Copper Oxide Cluster Ions Revealed by Post Heating. *J. Phys. Chem. A* **2013**, *117*, 10145−10150.

(18) Hirabayashi, S.; Ichihashi, M. Reactions of Size-Selected Copper Cluster Cations and Anions with Nitric Oxide: Enhancement of Adsorption in Coadsorption with Oxygen. *J. Phys. Chem. A* **2014**, *118*, 1761−1768.

(19) Mafuné, F.; Miyajima, K.; Morita, K. Release of Oxygen from Copper Oxide Cluster Ions by Heat and by Reaction with NO. *J. Phys. Chem. C* **2015**, *119*, 11106−11113.

(20) Jadraque, M.; Martín, M. DFT calculations of $Cu_nO_m{}^{0/+}$ clusters: Evidence for $Cu_2O$ building blocks. *Chem. Phys. Lett.* **2008**, *456*, 51−54.

(21) Dai, B.; Tian, L.; Yang, J. A theoretical study of small copper oxide clusters: $Cu_2O_x$ (x = 1−4). *J. Chem. Phys.* **2004**, *120*, 2746−2751.

(22) Bae, G.-T.; Dellinger, B.; Hall, R. W. Density Functional Calculation of the Structure and Electronic Properties of $Cu_nO_n$ (n = 1−8) Clusters. *J. Phys. Chem. A* **2011**, *115*, 2087−2095.

(23) Eiceman, G. A.; Karpas, Z.; Hill, H. H., Jr. *Ion Mobility Spectrometry*, 3rd ed.; CRC Press: New York, 2013.

(24) Bowers, M. T. Ion mobility spectrometry: A personal view of its development at UCSB. *Int. J. Mass Spectrom.* **2014**, *370*, 75−95.

(25) Lanucara, F.; Holman, S. W.; Gray, C. J.; Eyers, C. E. The power of ion mobility-mass spectrometry for structural character-ization and the study of conformational dynamics. *Nat. Chem.* **2014**, *6*, 281−294.

(26) Mason, E. A.; McDaniel, E. W. *Transport Properties of Ions in Gases*; Wiley and Sons: New York, 1988.

(27) Revercomb, H. E.; Mason, E. A. Theory of Plasma Chromatography/Gaseous Electrophoresis- A Review. *Anal. Chem.* **1975**, *47*, 970−983.

(28) Koyasu, K.; Komatsu, K.; Misaizu, F. Structural transition of zinc oxide cluster cations: Smallest tube like structure at $(ZnO)_6{}^+$. *J. Chem. Phys.* **2013**, *139*, 164308.

(29) Ota, K.; Koyasu, K.; Ohshimo, K.; Misaizu, F. Structures of cobalt oxide cluster cations studied by ion mobility mass spectrometry. *Chem. Phys. Lett.* **2013**, *588*, 63−67.

(30) Ohshimo, K.; Komukai, T.; Moriyama, R.; Misaizu, F. Isomer Separation of Iron Oxide Cluster Cations by Ion Mobility Mass Spectrometry. *J. Phys. Chem. A* **2014**, *118*, 3899−3905.

(31) Ohshimo, K.; Azuma, S.; Komukai, T.; Moriyama, R.; Misaizu, F. Structures and CO-Adsorption Reactivities of Nickel Oxide Cluster Cations Studied by Ion Mobility Mass Spectrometry. *J. Phys. Chem. C* **2015**, *119*, 11014−11021.

(32) Ohshimo, K.; Norimasa, N.; Moriyama, R.; Misaizu, F. Stable compositions and geometrical structures of titanium oxide clusters cations and anions studied by ion mobility mass spectrometry. *J. Chem. Phys.* **2016**, *144*, 194305.

(33) Wu, J. W. J.; Moriyama, R.; Tahara, H.; Ohshimo, K.; Misaizu, F. Compositions and Structures of Vanadium Oxide Cluster Ions $V_mO_n{}^\pm$ (m = 2−20) Investigated by Ion Mobility Mass Spectrometry. *J. Phys. Chem. A* **2016**, *120*, 3788−3796.

(34) Moriyama, R.; Sato, R.; Nakano, M.; Ohshimo, K.; Misaizu, F. Geometrical Structures of Gas Phase Chromium Oxide Cluster Anions Studied by Ion Mobility Mass Spectrometry. *J. Phys. Chem. A* **2017**, *121*, 5605−5613.

(35) Mesleh, M. F.; Hunter, J. M.; Shvartsburg, A. A.; Schatz, G. C.; Jarrold, M. F. Structural Information from Ion Mobility Measure-ments: Effects of the Long-Range Potential. *J. Phys. Chem.* **1996**, *100*, 16082−16086.

(36) Rusyniak, M. J.; Ibrahim, Y. M.; Wright, D. L.; Khanna, S. N.; El-Shall, M. S. Gas-Phase Ion Mobilities and Structures of Benzene Cluster Cations $(C_6H_6)_n{}^+$, n = 2−6. *J. Am. Chem. Soc.* **2003**, *125*, 12001−12013.

(37) Dugourd, Ph.; Hudgins, R. R.; Clemmer, D. E.; Jarrold, M. F. High-resolution ion mobility measurements. *Rev. Sci. Instrum.* **1997**, *68*, 1122−1129.

(38) Wu, J. W. J.; Moriyama, R.; Nakano, M.; Ohshimo, K.; Misaizu, F. Compositions and structures of niobium oxide cluster ions, $Nb_mO_n^{\pm}$, ($m = 2−12$), revealed by ion mobility mass spectrometry. *Phys. Chem. Chem. Phys.* **2017**, *19*, 24903−24914.

(39) Frisch, M. J.; Trucks, G. W.; Schlegel, H. B.; Scuseria, G. E.; Robb, M. A.; Cheeseman, J. R.; Scalmani, G.; Barone, V.; Mennucci, B.; Petersson, G. A.; et al. *Gaussian 09*, revision D.01; Gaussian, Inc.: Wallingford, CT, 2013.

(40) Cargnoni, G.; Kuś, T.; Mella, M.; Bartlett, R. J. Ground state potential energy surfaces and bound states of M-He dimers (M = Cu, Ag, Au): A theoretical investigation. *J. Chem. Phys.* **2008**, *129*, 204307.

(41) Partridge, H.; Stallcop, J. R.; Levin, E. Potential energy curves and transport properties for the interaction of He with other ground-state atoms. *J. Chem. Phys.* **2001**, *115*, 6471−6488.

(42) Batsanov, S. S. Van der Waals radii of elements. *Inorg. Mater.* **2001**, *37*, 871−885.

(43) Bondi, A. Van der Waals Volumes and Radii. *J. Phys. Chem.* **1964**, *68*, 441−451.

(44) Hirabayashi, S.; Ichihashi, M. Gas-Phase Reactions of Copper Oxide Cluster Cations with Ammonia: Selective Catalytic Oxidation to Nitrogen and water Molecules. *J. Phys. Chem. A* **2018**, *122*, 4801−4807.

(45) Bae, G. T. Structures and Electronic Properties of $Cu_3O_n$ ($n = 1−6$) Clusters using *ab initio* Monte Carlo Simulations. *Bull. Korean Chem. Soc.* **2016**, *37*, 638−642.